Archives of Acoustics Vol. 47, No. 4, pp. 529–538 (2022), doi: 10.24425/aoa.2022.142895

Research Paper

The Effect of a Concentrated Mass on the Acoustic Power and the Resonant Frequencies of a Circular Plate

Wojciech P. RDZANEK*, Krzysztof SZEMELA

University of Rzeszow, College of Natural Sciences, Institute of Physics
Rzeszow, Poland

*Corresponding Author e-mail: wordzanek@ur.edu.pl

(*received February 28, 2022; accepted July 4, 2022*)

This study presents an analysis of the effect of the concentrated mass on the acoustic power and the resonant frequencies of a vibrating thin circular plate. The fluid-structure interactions and the acoustic wave radiation effect have been included. The eigenfunction expansion has been used to express the transverse displacement of the plate. The appropriate number of modes is determined approximately to achieve physically correct results. Then highly accurate results are obtained numerically. The radiated acoustic power has been used to determine the resonant frequencies. The introducing of the concentrated mass is justified by modelling the added mass of the moving component of the exciter.

Keywords: thin plate; concentrated mass; fluid-structure interactions; resonant frequencies; modal expansion; acoustic power.

1. Introduction

An accurate determination of the resonant frequencies of vibrating structures is of the utmost importance in diagnostics and design both in mechanical engineering and physical systems. So far, a number of studies dealt with such problems. Some examples are the results proposed by Ostachowicz *et al.* (2002) who used a diagnostic method for localization of concentrated masses on a vibrating plate. They used the method of analysing the shifts in the resonant frequencies. Further, Cho *et al.* (2016) examined dynamic responses of stiffened panels with added masses and openings. Jun and Eom (1995) presented analytical results to the acoustic scattering from a circular aperture. They presented the acoustic pressure in the half-space in terms of the inverse Hankel transform. Rdzanek and Engel (2000) studied rigorously the acoustic power radiated by a single axisymmetric mode of a clamped annular plate. Zagrai and Donskoy (2005) studied analytically the natural frequencies of elastically supported circular plates. Rdzanek *et al.* (2007) examined rigorously the sound radiation from an elastically supported circular plate. They ignored the fluid-structure interactions. Arenas (2009) investigated the sound radiation from a circular hatchway. He used the model of an elastically supported circular plate for this purpose. Arenas and Ugarte (2016) analysed the behaviour of a circular panel sound absorber with an elastic boundary condition. Rdzanek (2018) examined rigorously the sound radiation from an elastically supported circular plate. He used the Zernike circle polynomials for this purpose. Rdzanek and Szemela (2019) applied the radial polynomials and the method spectral mapping to examine thoroughly the sound radiation from a vibrating annular plate. Lovat *et al.* (2019) presented a rigorous analysis of shielding capacity of a perfectly conducting circular disk. Hasheminejad and Keshavarzpour (2016) presented a robust active sound radiation control of a piezo-laminated composite circular plate. They used an exact elasticity model for a plate of arbitrary thickness. Hasheminejad and Shakeri (2017) studied a transient acoustic and structural response of a cavity-coupled circular plate system. They proposed a smart active control circuit. Wrona *et al.* (2020; 2021a; 2021b) analysed the effect of the added masses on shaping the dynamic responses of rectangular planar panels, semi-active links in double-panel noise barriers, and semi-active actuating for noise con-

trol applications. Trojanowski and Wiciak (2012; 2020), Wiciak and Trojanowski (2015) examined the effect of different piezo elements on vibration control of an elastic structure. They analysed the structure responses and the effect on the mode shapes. Jandak *et al.* (2017) presented the piezoelectric line moment actuator for active radiation control from some lightweight structures.

One of the methods of examining the frequency responses of structures is using the electro-magnetic exciters. The investigated structure is then excited within the desired frequency range and the normal vibration velocity is measured in selected points on the structure. The exciter needs to have sufficient force over the analysed frequency interval. Usually the mass of the moving component of the exciter is significant compared to mass of the structure. In such cases the effect of the added mass of the exciter on the resonant frequencies of the structures should not be neglected. This paper focuses on this problem. The examined structure is a thin circular plate. The plate is free at its circumferences and mounted at its centre to the exciter. This selection motivated by the simplicity of the structure and numerical analysis. The modal expansion of the plates vibrations is used along with the in-vacuo eigenfrequencies of the plate. Applying this expansion requires careful determination of all the necessary modes of the plate to achieve physically correct results. Therefore the non-dimensionalized added mass incrementals are determined to estimate roughly the resonant frequencies. Then some more modes will be taken for calculations to achieve the desired numerical accuracy. The proper and accurate determination of the resonant frequencies of structures is an important practical problem. Therefore some sample results are presented herein. In addition, the radiated acoustic power is obtained. This enables studying the effect of the added mass on the emitted noise. This study is organised as follows. First, the problem is solved analytically. Next, the numerical results are presented and discussed. The final conclusions are drawn. The appendices present selected equations useful for numerical calculations. Although the free vibrations have been presented in the literature so far, they have been shown here in appendixes for convenience. In addition, the frequency equation and the eigenfunctions have been presented in a more clear way than earlier by Rdzanek (2018). Therefore, these data are useful for numerical calculations presented in this study.

2. Governing equations

2.1. Statement of the problem

The problem of sound radiation by a circular plate is embedded in the flat rigid screen at the plane $z = 0$ (cf. Fig. 1). The thickness and the density of the plate are then h and ϱ, respectively. The plate is driven by an electromagnetic exciter (or by a system of L exciters). The entire space around the plate is filled with air of ambient density ϱ_0 [kg · m^{-3}]. The speed of sound in air is c [m · s^{-1}]. The plate vibrates and radiates acoustic waves into both half spaces, the upper and the lower. The cylindrical coordinates (r, ϕ, z) are used. Consequently, the position vector is $\mathbf{r} = (r, \phi, z)$. The plate is excited for steady time harmonic vibrations. The time dependence $\mathrm{e}^{-\mathrm{i}\omega t}$ has been suppressed throughout the entire analysis, where $\mathrm{i}^2 = -1$, $\omega = kc$ is the angular frequency [rad · s^{-1}], $k = 2\pi/\Lambda$ [rad · m^{-1}] is the wavenumber in air, while Λ is the corresponding wavelength, and t stands for time [s].

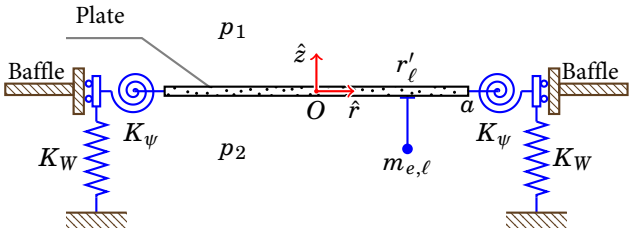

Fig. 1. Geometry of the problem of a vibrating circular plate elastically supported at its circumference. The plate is embedded into a flat rigid baffle. In addition, a concentrated mass is attached to the plate at the polar coordinates (r', ϕ').

The considered system is governed by the system of the three coupled differential equations. They are the following two Helmholtz equations and the equation of motion of the excited plate (e.g. (Rao, 2007), Eq. (14.200), and (Ostachowicz, 2002)):

$$\left(\nabla^2 + k^2\right)p_1(r,\phi,z) = 0,$$

$$\left(\nabla^2 + k^2\right)p_2(r,\phi,z) = 0,$$

$$D\nabla^4 W(r,\phi) - \varrho h\omega^2 W(r,\phi) - \omega^2 \sum_{\ell=1}^{L} m_{e,\ell}\frac{\delta(r-r'_\ell)}{r}\delta(\phi-\phi'_\ell)W(r,\phi) + 2p(r,\phi,0) = P(r,\phi), \tag{1}$$

where k_D [rad/m] is the complex bending wavenumber, $k_D^4 = \omega^2\varrho h/D$, $D_E = Eh^3/[12(1-\nu^2)]$, η is the plate's damping coefficient, $D = D_E(1 + \mathrm{i}\eta)$ is the complex bending stiffness (cf. Appendix A), $m_{e,\ell}$ is the mass of the moving component of the ℓ-th exciter concentrated on the plate at $(r'_\ell,\ \phi'_\ell)$, $\delta(r - r'_\ell)$ [m^{-1}], and $\delta(\phi - \phi'_\ell)$ [rad^{-1}] are the Dirac deltas, $P(r,\phi)$ [Pa] is the external excitation (force per surface area), $p_1(r,\phi,z)$ is the acoustic pressure in the lower half-space, $p_2(r,\phi,z)$ is the acoustic pressure in the upper half-space, $2p(r,\phi,z) = p_1(r,\phi,z) - p_2(r,\phi,-z)$ (also $p(r,\phi,z) = p_1(r,\phi,z) = -p_2(r,\phi,-z)$ due to inverse symmetry of the acoustic field with respect to the plane $z = 0$), the Laplace's operator is

$\nabla^2 = \frac{1}{r}\frac{\partial}{\partial r}\left(r\frac{\partial}{\partial r}\right)+\frac{1}{r^2}\frac{\partial^2}{\partial\phi^2}+\frac{\partial^2}{\partial z^2}$, and the biharmonic operator is $\nabla^4 = \nabla^2\nabla^2$. The concentrated masses $m_{e,\ell}$ have been introduced to include the effect of the masses of the moving components of the exciters on the vibrations of the plate (cf. (Ostachowicz, 2002) Eq. (2)). Consequently, the third term in Eq. $(1)_3$ represents the inertial forces. In addition, the following Neumann boundary condition has to be satisfied:

$$\frac{1}{\mathrm{i}\omega\varrho_0}\frac{\partial p_\mu}{\partial z}\bigg|_{z=0} = \begin{cases} v(r,\phi); & 0 \leqslant r \leqslant a, \\ 0; & \text{otherwise}, \end{cases} \tag{2}$$

for $\mu = 1, 2$.

2.2. Solving the Helmholtz equation

The acoustic pressure and the normal vibration velocity can be predicted in the following form (cf. (Jun, Eom, 1995), Eqs (1)–(3)):

$$\begin{aligned} p(r,\phi,z) &= \sum_m \mathrm{e}^{\mathrm{i}m\phi}\int_0^\infty f^m(\tau)J_{|m|}(\tau r)\mathrm{e}^{\mathrm{i}K|z|}\frac{\tau\,\mathrm{d}\tau}{K}, \\ v(r,\phi) &= -\mathrm{i}\omega W(r,\phi), \\ W(r,\phi) &= \sum_m \mathrm{e}^{\mathrm{i}m\phi}\sum_s c_s^m W_s^{|m|}(r), \\ \frac{\delta(r-r'_\ell)}{r}\delta(\phi-\phi'_\ell) &= \frac{1}{S_a}\sum_m \mathrm{e}^{\mathrm{i}m(\phi-\phi'_\ell)} \\ &\quad\cdot\sum_s W_s^{|m|}(r)W_s^{|m|}(r'_\ell), \end{aligned} \tag{3}$$

for $|m|, n, s = 0, 1, 2, \ldots$, where $\mathbf{r} = (r,\phi,z)$ is the field point vector, k is the wavenumber, $K^2 = k^2 - \tau^2$, $v(r,\phi)$ is the normal component of the plate's vibration velocity, $W(r,\phi)$ is the plate's transverse deflection, and $W_s^{|m|}(r)\mathrm{e}^{\mathrm{i}m\phi}$ is the plate's eigenfunction (cf. Appendix A). The acoustic pressures p_2 in Eq. $(3)_1$ radiated into the upper half-space are expressed as the Rayleigh first integral (cf. (Rayleigh, 1896) Sec. 278; (Williams, 1999) Eq. (2.75); (Pierce, 1994) Eq. (5–2.1)). It also satisfies the radiation condition (cf. (Sommerfeld, 1964), Sec. 28, p. 189, Eq. (2)) $\lim_{R\to\infty} R\left(\frac{\partial p}{\partial R} - \mathrm{i}kp\right) = 0$, where $R = |\mathbf{r}| = (r^2+z^2)^{1/2}$.

Inserting Eq. $(3)_1$ to the boundary condition in Eq. (2) leads to (cf. Eqs $(27)_2$ and (29)):

$$f^m(\tau) = -\mathrm{i}\omega^2\varrho_0\sum_s c_s^m\widehat{D}_s^{|m|}(\tau). \tag{4}$$

Then, applying Eq. (4) back to Eq. $(3)_1$ gives:

$$p(r,\phi,z) = \omega^2\varrho_0\sum_m \mathrm{e}^{\mathrm{i}m\phi}\sum_s c_s^m\widehat{p}_s^{|m|}(r,z), \tag{5}$$

where

$$\widehat{p}_s^{|m|}(r,z) = -\mathrm{i}\int_0^\infty \widehat{D}_s^{|m|}(\tau)J_{|m|}(\tau r)\mathrm{e}^{\mathrm{i}K|z|}\frac{\tau\,\mathrm{d}\tau}{K}. \tag{6}$$

2.3. Excited vibrations of the plate

The external excitation can be expressed as follows:

$$P(r,\phi) = \sum_m \mathrm{e}^{\mathrm{i}m\phi}\sum_s \widehat{P}_s^m W_s^{|m|}(r), \tag{7}$$

where the expansion coefficients are (Eq. $(29)_1$):

$$\widehat{P}_s^m = \frac{1}{S_a}\int_{-\pi}^{+\pi}\int_0^a P(r,\phi)W_s^{|m|}(r)\mathrm{e}^{-\mathrm{i}m\phi}r\,\mathrm{d}r\,\mathrm{d}\phi. \tag{8}$$

Different excitations have described in detail earlier by Rdzanek and Szmela (2019) (cf. their Sec. II.D and App. D). The two most useful excitations are the point excitation and the uniform excitation on a circle. They can be formulated as follows:

$$\begin{aligned} P_{\text{poi.}}(r,\phi) &= S_a\sum_{\ell=1}^L P_{0,\ell}\frac{\delta(r-r'_\ell)}{r}\delta(\phi-\phi'_\ell); \quad 0 \leqslant r'_\ell < a, \\ P_{\text{circ.}}(r,\phi) &= \sum_{\ell=1}^L P_{0,\ell}\frac{S_a}{S_{0,\ell}}\begin{cases} 1; & 0 \leqslant r_{0,\ell} \leqslant a_{0,\ell}, \\ 0; & \text{otherwise}, \end{cases} \end{aligned} \tag{9}$$

where $P_{0,\ell}$ is the excitation amplitude, $S_a = \pi a^2$, $S_{0,\ell} = \pi a_{0,\ell}^2$, (r'_ℓ,ϕ'_ℓ) are the polar coordinates of the excitation centre of the ℓ-th exciter, $(r_{0,\ell},\phi_{0,\ell})$ are the local polar coordinates. Equation $(9)_1$ represents the point excitation and Eq. $(9)_2$ represents the circular excitation. The modal excitation coefficients can be obtained by substituting the above equations into Eq. (8):

$$\begin{aligned} \widehat{P}_{\text{poi.},s}^m &= \sum_{\ell=1}^L P_{0,\ell}W_s^{|m|}(r'_\ell)\mathrm{e}^{-\mathrm{i}m\phi'_\ell}; \quad 0 < r'_\ell < a, \\ \widehat{P}_{\text{circ.},s}^m &= \sum_{\ell=1}^L P_{0,\ell}\widehat{W}_s^{|m|}(r'_\ell,a_{0,\ell})\mathrm{e}^{-\mathrm{i}m\phi'_\ell}; \\ &\qquad 0 \leqslant r'_\ell < a - a_{0,\ell}, \end{aligned} \tag{10}$$

where

$$\begin{aligned} \widehat{W}_s^{|m|}(r'_\ell,a_{0,\ell}) &= \widehat{N}_s^{|m|}\Bigg\{J_{|m|}(k_s^{|m|}r'_\ell)\frac{2J_1(k_s^{|m|}a_{0,\ell})}{k_s^{|m|}a_{0,\ell}} \\ &\quad + B_s^{|m|}I_{|m|}(k_s^{|m|}r'_\ell)\frac{2I_1(k_s^{|m|}a_{0,\ell})}{k_s^{|m|}a_{0,\ell}}\Bigg\}, \end{aligned} \tag{11}$$

and $\lim_{a_{0,\ell}\to 0}\widehat{W}_s^{|m|}(r'_\ell,a_{0,\ell}) = W_s^{|m|}(r'_\ell)$.

Further, substituting Eqs $(3)_1$–$(3)_3$, (5)–(7), into the equation of motion of the plate in Eq. $(1)_3$ provides (cf. Eqs (23), (25), and $(29)_1$):

$$\begin{aligned} c_{s'}^{m'}\left(\frac{(k_{s'}^{|m'|})^4}{k_D^4} - 1\right) - 2\mathrm{i}\frac{\varrho_0}{\varrho kh}\sum_s c_s^{m'}\widehat{\zeta}_{ss'}^{|m'|} \\ - \sum_m\sum_s c_s^m\widehat{\xi}_{ss',\ell}^{mm'} = \frac{\widehat{P}_{s'}^{m'}}{\omega^2\varrho h}, \end{aligned} \tag{12}$$

where the modal radiation impedance and the concentrated mass coefficients are (cf. (Rdzanek, Szmela, 2019) Eq. (14a)):

$$\widehat{\zeta}_{ss'}^{|m|} = \frac{2k}{a^2}\int_0^{\infty}\widehat{D}_s^{|m|}(\tau)\widehat{D}_{s'}^{|m|}(\tau)\frac{\tau\,\mathrm{d}\tau}{K},$$
$$\widehat{\xi}_{ss',\ell}^{mm'} = \sum_{\ell=1}^{L}\frac{m_{e,\ell}}{m_p}W_s^{|m|}(r'_\ell)W_{s'}^{|m'|}(r'_\ell)\mathrm{e}^{\mathrm{i}(m-m')\phi'_\ell}, \tag{13}$$

and $m_p = \varrho h S_a$ is the mass of the plate. Although the integral in Eq. $(13)_1$ presupposes troublesome numerical calculations, it can be accurately and efficiently evaluated using the circle Zernike polynomials (cf. (Rdzanek, 2019) Eqs (14a)–(14c)).

2.4. Acoustic power

The total time averaged reference acoustic power from the vibrating plate is

$$\Pi_{\mathrm{ref}} = \varrho_0 c S_a\left\langle|v(r,\phi)|^2\right\rangle, \tag{14}$$

where $|v(r,\phi)|^2 = v(r,\phi)v^*(r,\phi)$, $S_a = \pi a^2$ is the surface of the plate, the mean square velocity on the plate is (cf. Eqs $(3)_1$, (25), and $(29)_1$):

$$\left\langle|v(r,\phi)|^2\right\rangle = \frac{1}{S_a}\int_{-\pi}^{+\pi}\int_0^a|v(r,\phi)|^2 r\,\mathrm{d}r\,\mathrm{d}\phi = \omega^2\sum_m\sum_s|c_s^m|^2, \tag{15}$$

where $|c_s^m|^2 = c_s^m c_s^{m*}$. The time averaged acoustic powers radiated is (cf. Eqs $(3)_1$–$(3)_3$, $(27)_2$, and $(29)_1$):

$$\begin{aligned}\Pi &= \int_{-\pi}^{+\pi}\int_0^a \mathrm{Re}\Big\{p(r,\phi,0)v^*(r,\phi)\Big\}r\,\mathrm{d}r\,\mathrm{d}\phi\\ &= \varrho_0 c\omega^2 S_a\sum_m\sum_s\sum_{s'}\mathrm{Re}\Big(c_s^m\widehat{\zeta}_{ss'}^{|m|}c_{s'}^{m*}\Big),\end{aligned} \tag{16}$$

where it has been accepted that $u_z(r,\phi,0) = v(r,\phi)$ on the basis on the Huygens principle (in the case of the non-homogeneous Neumann boundary condition). Note that the expression in Eq. (16) represents the acoustic power radiated by both sides of the plate. The radiation efficiency is

$$\sigma = \frac{\Pi}{\Pi_{\mathrm{ref}}}. \tag{17}$$

2.5. Acoustic pressure on the plate

The acoustic pressure modal coefficient in Eq. (6) on the plate can be rearranged using the following expansion (cf. Eqs (25) and $(27)_2$):

$$J_{|m|}(\tau r) = \frac{2}{a^2}\sum_s\widehat{D}_s^{|m|}(\tau)W_s^{|m|}(r), \tag{18}$$

for $z = 0$ and $r \leqslant a$. Now, applying Eq. (18) to Eq. (6) yields (cf. Eq. $(13)_1$):

$$\widehat{p}_s^{|m|}(r,0) = -\frac{\mathrm{i}}{k}\sum_{s'}\widehat{\zeta}_{ss'}^{|m|}W_{s'}^{|m|}(r). \tag{19}$$

2.6. Added mass incremental factors

Now, taking only the dominant mode $(|m|,s)$ in Eq. (12) gives the following equations with the added mass and the fluid loading and without it, respectively:

$$\begin{aligned}c_{1,s}^m\Bigg(&D(k_s^{|m|})^4 - \omega_1^2\varrho h - 2\omega_1^2\varrho h\frac{\varrho_0}{\varrho h}\mathrm{Re}(\mathrm{i}\widehat{\zeta}_{ss}^{|m|}/k_1)\\ &-\omega_1^2\varrho h\sum_{\ell=1}^{L}\frac{m_{e,\ell}}{m_p}[W_s^{|m|}(r'_\ell)]^2\Bigg) = \widehat{P}_s^m,\\ c_{2,s}^m&\Big(D(k_s^{|m|})^4 - \omega_2^2\varrho h\Big) = \widehat{P}_s^m,\end{aligned} \tag{20}$$

where $\omega_1 = k_1 c$ is the resonant frequency for $m_{e,\ell} \neq 0$ and ω_2 is the resonant frequency for $m_{e,\ell} = 0$. Then, accepting the approximation than $c_{1,s} \simeq c_{2,s}$ and comparing these two equations side by side leads to:

$$\omega_1 \simeq \frac{\omega_2}{\sqrt{1+\beta_{f,s}^{|m|}+\beta_{e,s}^{|m|}}}, \tag{21}$$

since $\mathrm{Re}(\mathrm{i}\widehat{\zeta}_{ss}^{|m|}/k_1) = -\mathrm{Im}(\widehat{\zeta}_{ss}^{|m|}/k_1)$, where the added virtual mass incremental (AVMI) factors are:

$$\begin{aligned}\beta_{f,s}^{|m|} &= -2\frac{\varrho_0}{\varrho h}\mathrm{Im}\left(\widehat{\zeta}_{ss}^{|m|}/k_1\right),\\ \beta_{e,s}^{|m|} &= \widehat{\xi}_{ss,\ell}^{mm} = \sum_{\ell=1}^{L}\frac{m_{e,\ell}}{m_p}[W_s^{|m|}(r'_\ell)]^2,\end{aligned} \tag{22}$$

and $\beta_{f,s}^{|m|}, \beta_{e,s}^{|m|} \geqslant 0$. The first of the two factors occurs due to the fluid-structure interactions, while the second one due to the attached concentrated masses $m_{e,\ell}$. Any of the two factors can be neglected, when it is much smaller than unity. Although, the resonant wavenumber k_1 is not known a priori, the calculations for $\beta_{f,s}^{|m|}$ can be iterated as many times as the sufficient accuracy is achieved (note also that $\widehat{\zeta}_{ss}^{|m|} = \widehat{\zeta}_{ss'}^{|m|}(k_1)$).

3. Numerical analysis

The numerical analysis has been performed by assuming the arbitrary parameter values such as: the speed of sound in air $c = 343\ \mathrm{m\cdot s^{-1}}$, the density of air $\varrho_0 = 1.2\ \mathrm{kg\cdot m^{-3}}$, the radius of the plate $a = 150$ mm, the radius of the excitation $a_0 = 6.5$ mm, the thickness of the plate $h = 1$ mm, the Young's modulus $E = 210\cdot 10^9$ Pa, the damping coefficient $\eta = 10^{-2}$, the density of steel $\varrho = 7850\ \mathrm{kg\cdot m^{-3}}$, the Poisson ratio $\nu = 0.30$, the external excitation amplitude $F_e = 1$ N $(P_0 = F_e/S_0)$,

the excitation radial coordinate $0 \leqslant r' < a$, and the excitation angular coordinate that has been selected arbitrarily. More specifically, the following values have been used for calculations $r'/a = 0$, 0.25, 0.5 and 0.75. The majority of results is shown for $r'/a = 0.75$ because they give a strongly asymmetric excitation and results in strong maxima at the many resonant frequencies. For $r'/a = 0$, we have simply the axisymmetric excitation and the maxima occur only for the axisymmetric resonant frequencies. The angular localization of the excitation point does not effect the SWL and the radiation efficiency when a single exciter is used. In the case of many exciters, their angular localization should be taken into account. All the analysis presented herein has been performed for a single exciter, which does not reduce the generality of the results presented. The normalized boundary stiffness values are $\overline{K}_W = 10^9$ and $\overline{K}_\psi = 10^9$. Such great values of the stiffnesses have been selected to approximate the clamped edge boundary conditions.

Figure 2a shows the sound Watt level (SWL) radiated by a vibrating plate with an attached mass m_e. This figure reveals that increasing the mass m_e causes a significant decrease of the fundamental resonant frequency. This is because the increasing AVMI factor is associated with this mass according to Eq. (21). The higher resonant frequencies show the same tendency. In addiction, the SWL is also significantly decreased. This is important for practical noise control applications. Figure 2b shows that an increase in the mass has a negligibly small effect on the radiation efficiency.

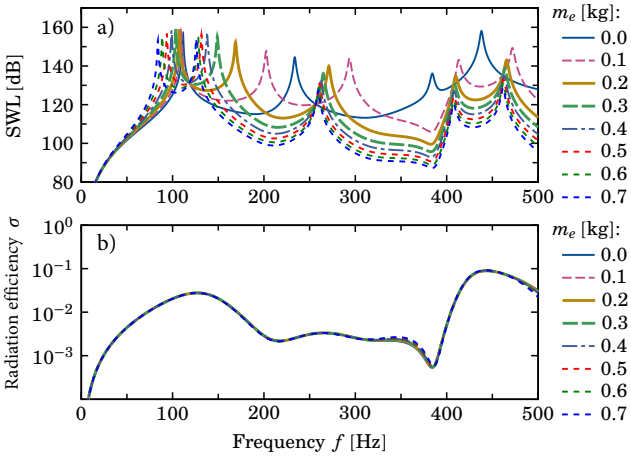

Fig. 2. a) Shows the SWL [dB, Ref. 1 pW] radiated from a vibrating circular plate for different values of the mass m_e attached to the plate, b) shows the radiation efficiency σ for $r'/a = 0.75$ and different values of m_e.

Finding the values of the coefficients $c_s^{|m|}$ in Eq. $(3)_3$ requires solving numerically the system of algebraic equations in Eq. (12). First, the number of necessary modes should be determined. It is required that the modes of eigenfrequencies smaller than the driving frequency should be included to assure physically correct results. This means that the summation limits in Eq. $(3)_3$ are $|m| = 0, ..., M-1$ and $s = 0, ..., S-1$, where M and S are the maximal modal numbers. Nevertheless, achieving a desired accuracy requires increasing those maximal numbers by an incremental ΔS, which leads to the actual maximal modal numbers $M + \Delta S$ and $S + \Delta S$ being used in numerical calculations. While M and S are determined by the driving frequency f, the incremental ΔS can be increased arbitrarily to achieve better accuracy. Figure 3a shows the effect of the incremental ΔS on the SWL. All the curves are essentially the same regardless the value of ΔS. Figure 3b shows the relative difference $\delta\Pi = 100|\Pi - \Pi_{\mathrm{Ref}}|/|\Pi_{\mathrm{Ref}}|\,(\%)$ of the acoustic power Π, where the reference value Π_{Ref} has been obtained for $\Delta S = 50$. The greater is ΔS, the better the accuracy. The difference does not exceed 10 % for frequencies smaller than 250 Hz and $\Delta S \geqslant 10$, except for the resonant frequencies where the growth in the difference can be noticed. This growth will be examined more closely later on. The relative difference for the radiation efficiency and the reference values is presented in Fig. 3c. It does not exceed 1% for frequencies smaller than 500 Hz and $\Delta S \geqslant 10$.

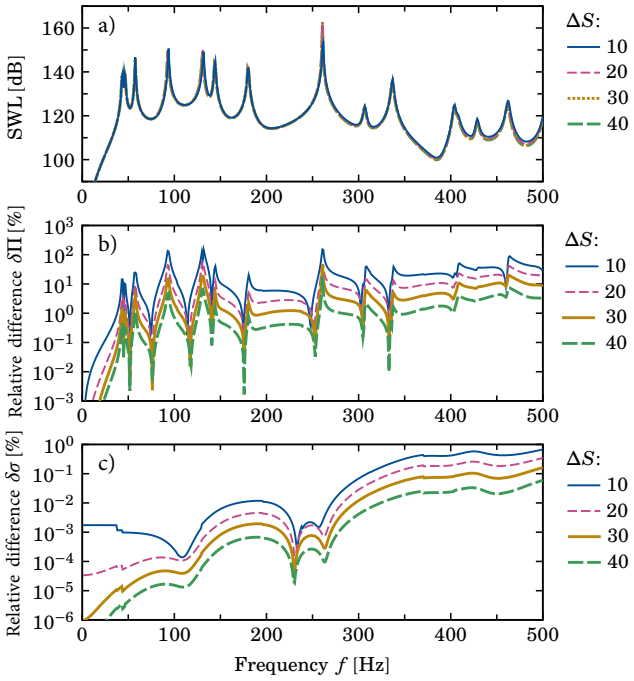

Fig. 3. a) Shows the SWL [dB, Ref. 1 pW] radiated from a vibrating circular plate, b) shows the relative difference $\delta\Pi$ [%] between the results obtained for different values of ΔS and the reference obtained for $\Delta S = 50$, and c) shows the relative difference $\delta\sigma$ [%] for $m_e = 0.5$ kg and $r'/a = 0.75$.

Figure 4 illustrates the effect of the mass of the moving component of the exciter. By increasing the mass

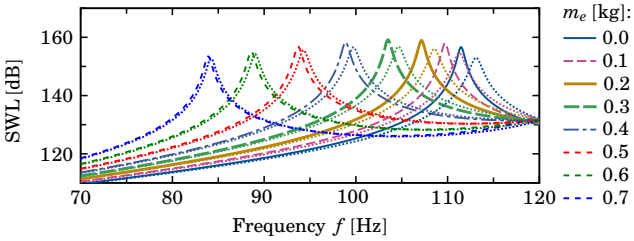

Fig. 4. SWL [dB, Ref. 1 pW] radiated from a vibrating circular plate for different values of the mass m_e attached to the plate for $m_e = 0.5$ kg and $r'/a = 0.75$. The dotted curves illustrate the case when the fluid loading is neglected in calculations.

from 0 up to 0.7 kg, the fundamental resonant frequency has been caused to decrease from about 112 Hz to about 88 Hz. The decrease is then about 24 Hz. The dotted lines show the acoustic power with the fluid loading effect neglected. The resonant maxima are slightly higher than those with the fluid loading included. The greater is the mass of the exciter, the smaller is the shift due to fluid loading.

Figure 5a shows the effect of the incremental ΔS on the fundamental resonant frequency for $m_e = 0.5$ kg. The maxima nearly overlap for $\Delta S \geqslant 20$, while for $\Delta S = 10$ the frequency is higher by about 1 Hz. The SWL values are nearly identical for all analysed values

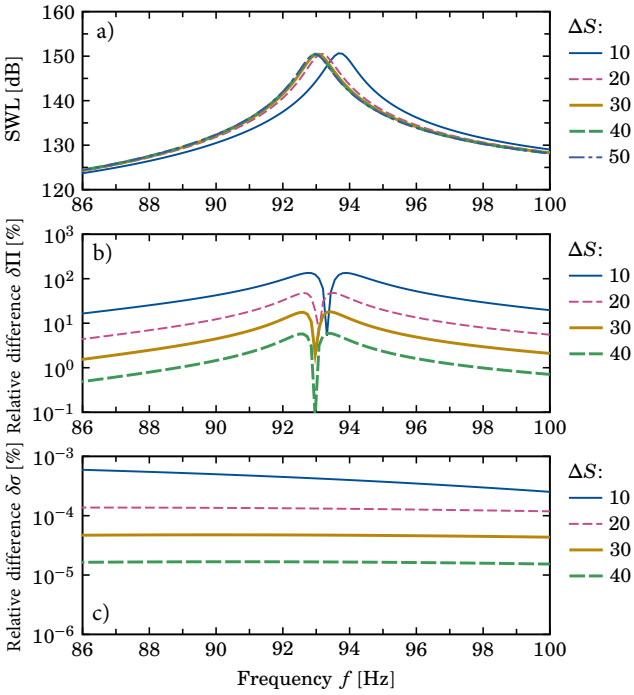

Fig. 5. a) Shows the SWL [dB, Ref. 1 pW] radiated from a vibrating circular plate, b) shows the relative difference $\delta\Pi$ [%] between the results obtained for different values of ΔS and the reference obtained for $\Delta S = 50$, and c) shows the relative difference $\delta\sigma$ [%] for $m_e = 0.5$ kg and $r'/a = 0.75$.

of ΔS. This means that if accuracy of ±1 Hz is acceptable, then $\Delta S = 10$ is sufficient. If a greater accuracy is required, then ΔS should be at least 20. This shift in frequency causes the growth in the relative error, which is shown in Fig. 5b. This does not significantly affect the SWL value at the resonant maximum. Figure 5c shows that the relative difference for the radiation efficiency is negligibly small around the fundamental resonant frequency.

Figure 6 shows the relative difference as a function of ΔS. The difference decreases rapidly with the growth in ΔS. This means that the quantity converges to the reference value.

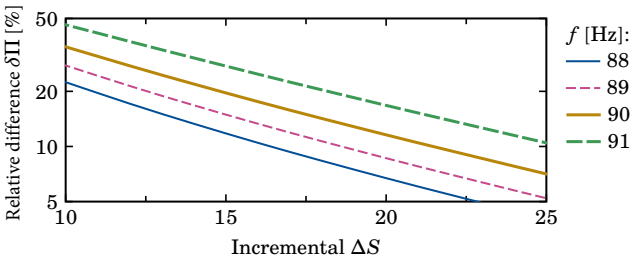

Fig. 6. Relative difference $\delta\Pi$ [%] as a function of ΔS for different frequencies f. The reference values have been obtained for $\Delta S = 50$ for $m_e = 0.5$ kg and $r'/a = 0.75$.

Figure 7 illustrates the effect of the localization of the exciter on the SWL and the radiation efficiency. This effect is significant. Figure 7a shows that increasing the radial variable r' of the localization results in shifting the fundamental frequency of the vibrating system towards higher frequencies. The SWL is increased or decreased depending on the frequency of excitation. In the case of the radiation efficiency presented in Fig. 7b, there is nearly no effect for frequencies smaller than 100 Hz. However, significant differences can be observed for higher frequencies.

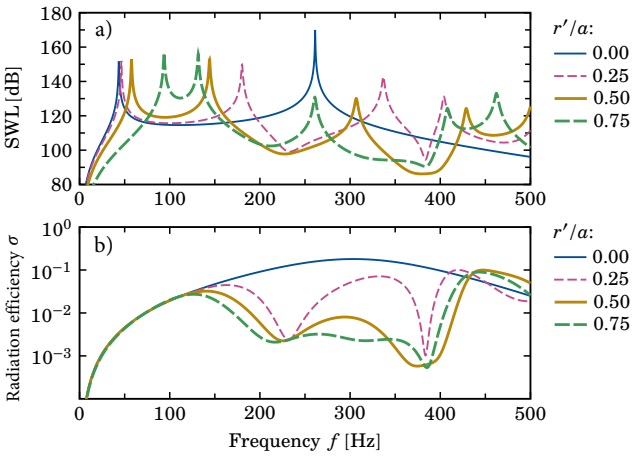

Fig. 7. a) Shows the SWL [dB, Ref. 1 pW] radiated from a vibrating circular plate, b) shows the radiation efficiency σ for $m_e = 0.5$ kg and different values of r'/a.

4. Concluding remarks

It has been shown that the concentrated mass attached to a vibrating circular plate significantly reduces its fundamental resonant frequency. At the same time, the sound Watt level at the resonant maximum is only weakly altered. The higher resonant frequencies behave similarly. The localization of the mass of the exciter is also important in this respect. The radiation efficiency is not significantly affected by adding the mass. The problem has been solved analytically using the modal based approach. The real modes of the coupled plate-mass system have been expressed by a series of the in-vacuo eigenfunctions of the plate. This leads to approximated results. If an insufficient number of modes is applied, then the resonant frequencies can be determined with a weaker accuracy. The frequencies can be read either from the mean square vibration velocity or from the active acoustic power plots. The discrepancy is about 1 Hz. If a higher accuracy is required, the number of modes applied should be increased. It is useful for numerical modelling to add a concentrated mass to a vibrating circular plate, as the mass can represent the moving component of the exciter. In addition, it can be significant compared to the mass of the plate. Although, it was to be expected based on the literature data, a purely analytical approach has been presented herein for a circular plate. The numerical results obtained this way can be helpful for designing a real system containing such vibrating plates.

Acknowledgments

The research presented in this paper was partially supported within the Centre for Innovation and Transfer of Natural Sciences and Engineering Knowledge Project at the University of Rzeszów in Poland.

Appendix A. Free vibrations of the plate

The free vibrations of the plate are governed by the following biharmonic equation (cf. (Rao, 2007) Eq. (14.203)):

$$\nabla^4 W_s^{|m|}(r)\mathrm{e}^{\mathrm{i}m\phi} = (k_s^{|m|})^4 W_s^{|m|}(r)\mathrm{e}^{\mathrm{i}m\phi}, \tag{23}$$

for $|m|, s = 0, 1, 2, ...$, where $W_s^{|m|}(r)\mathrm{e}^{\mathrm{i}m\phi}$ is the plate's eigenfunction. The radial component of the plate's eigenfunction can be expressed as follows (cf. (McLachlan, 1995) p. 162 Eqs (78) and (79), p. 164 Eq. (108), and p. 166 Eq. (132)):

$$W_s^{|m|}(r) = \widehat{N}_s^{|m|}\Big[J_{|m|}(k_s^{|m|}r) + B_s^{|m|}I_{|m|}(k_s^{|m|}r)\Big], \tag{24}$$

for $0 \leqslant r \leqslant a$ and zero otherwise, where the normalization constant $\widehat{N}_s^{|m|}$ is presented in Eq. (28), $|m|$ enumerates the nodal diameters, n the nodal circles (cf. (Rao, 2007) p. 493), the prime sign denotes differentiation over the entire argument, $I_{|m|}(\lambda)$ is the modified Bessel function, $\widehat{N}_s^{|m|}$ and $\widehat{B}_s^{|m|}$ are the unknown constants; $k_s^{|m|}$ [rad/m] is the bending wavenumber of the mode $(|m|, s)$; $(k_s^{|m|})^4 = (\omega_s^{|m|})^2\varrho h/D_E$; $\omega_s^{|m|}$ is the angular eigenfrequency; $D_E = Eh^3/[12(1-\nu^2)]$ is the plate's stiffnesses; ϱ and h are the density and thickness; and E and ν are the Young modulus and the Poisson ratio. The radial components of the eigenfunctions satisfy the following orthogonality relation:

$$\int_0^a W_s^{|m|}(r)W_{s'}^{|m|}(r)r\,\mathrm{d}r = \frac{S_a}{2\pi}\delta_{ss'}, \tag{25}$$

where $\delta_{ss'}$ is the Kronecker delta, and $S_a = \pi a^2$.

The plate's eigenfunction $W \equiv W_s^{|m|}(r)\mathrm{e}^{\mathrm{i}m\phi}$ satisfies the following boundary conditions (cf. Fig. 4 and (Rao, 2007) Eqs (14.191) and (14.192)):

$$\begin{aligned} &K_W W(a,\phi) - D_E\left[\frac{\partial}{\partial r}\left(\nabla^2 W\right)\right. \\ &\qquad\left. + \frac{1-\nu}{r}\frac{\partial}{\partial r}\left(\frac{1}{r}\frac{\partial^2 W}{\partial\phi^2}\right)\right]_{r=a} = 0, \\ &K_\psi \left.\frac{\partial W}{\partial r}\right|_{r=a} + D_E\left[\frac{\partial^2 W}{\partial r^2}\right. \\ &\qquad\left. + \nu\left(\frac{1}{r}\frac{\partial W}{\partial r} + \frac{1}{r^2}\frac{\partial^2 W}{\partial\phi^2}\right)\right]_{r=a} = 0, \end{aligned} \tag{26}$$

It is convenient to present the radial component in Eq. (24) as equal to zero for any value of r except for $0 \leqslant r \leqslant a$, because it enables us to express the transverse deflection of the plate as well as its spectral density in terms of the Hankel transforms:

$$\begin{aligned} W_s^{|m|}(r) &= \int_0^\infty \widehat{D}_s^{|m|}(\tau)J_{|m|}(\tau r)\tau\,\mathrm{d}\tau, \\ \widehat{D}_s^{|m|}(\tau) &= \int_0^a W_s^{|m|}(r)J_{|m|}(\tau r)r\,\mathrm{d}r. \end{aligned} \tag{27}$$

The normalization constant can be obtained directly from Eq. (25) by substituting $s = s'$ (cf. (Rdzanek, Engel, 2000)):

$$(\widehat{N}_s^{|m|})^{-2} = \frac{2}{a^2}\int_0^a \Big[J_{|m|}(k_s^{|m|}r) + B_s^{|m|}I_{|m|}(k_s^{|m|}r)\Big]^2 r\,\mathrm{d}r. \tag{28}$$

The following integral relations are also useful:

$$\begin{aligned} \frac{1}{2\pi}\int_{-\pi}^{+\pi}\mathrm{e}^{\mathrm{i}(m-m')\phi}\,\mathrm{d}\phi &= \delta_{mm'}, \\ \int_0^\infty J_{|m|}(\tau r)J_{|m|}(\tau' r)r\,\mathrm{d}r &= \frac{\delta(\tau-\tau')}{\tau'}. \end{aligned} \tag{29}$$

Appendix B. Eigenfunctions of the plate

B.1. The characteristic equation

The characteristic equation of a thin elastically supported circular plate together with the constants $\widehat{N}_s^{|m|}$ and $\widehat{B}_s^{|m|}$ has been presented earlier (cf. (Leissa, 1969) Sec. 2.1.4, (Zagrai, Donskoy, 2005) Eqs (7)–(10), (Rdzanek, 2018) Eqs (25a) and (25b)). Nevertheless, they are reviewed below briefly and presented in the form which is useful for numerical calculations.

Inserting Eq. (24) into (26) yields (cf. Eq. $(27)_1$):

$$\begin{aligned} &q^{|m|}(\lambda)\Big[J_{|m|}(\lambda)+B_s^{|m|}I_{|m|}(\lambda)\Big]\\ &+\Big[2-u_{|m|}(\lambda)\Big]J'_{|m|}(\lambda)-u_{|m|}(\lambda)B_s^{|m|}I'_{|m|}(\lambda)=0,\\ &p^{|m|}(\lambda)\Big[J'_{|m|}(\lambda)+B_s^{|m|}I'_{|m|}(\lambda)\Big]-u_{|m|}(\lambda)J_{|m|}(\lambda)\\ &\qquad+\Big[2-u_{|m|}(\lambda)\Big]B_s^{|m|}I_{|m|}(\lambda)=0, \end{aligned} \tag{30}$$

for $\lambda = k_s^{|m|}a$ (here and in the entire appendix, unless stated otherwise), where

$$\begin{aligned} &q^{|m|}(\lambda)=\frac{1}{\lambda^3}\Big[+\overline{K}_W-(1-\nu)m^2\Big],\quad \overline{K}_W=\frac{K_W a^3}{D_E},\\ &p^{|m|}(\lambda)=\frac{1}{\lambda}\Big[+\overline{K}_\psi-(1-\nu)\Big],\qquad \overline{K}_\psi=\frac{K_\psi a}{D_E},\\ &u_{|m|}(\lambda)=1-(1-\nu)\frac{m^2}{\lambda^2}. \end{aligned} \tag{31}$$

The Bessel and the modified Bessel equations have been used (cf. (Abramowicz, Stegun, 1972) Eqs (9.1.1) and (9.6.1)):

$$\begin{aligned} &\left[\frac{1}{r}\frac{\partial}{\partial r}\left(r\frac{\partial}{\partial r}\right)-\frac{m^2}{r^2}\right]\begin{Bmatrix}J_{|m|}(k_s^{|m|}r)\\ I_{|m|}(k_s^{|m|}r)\end{Bmatrix}\\ &\qquad=\mp(k_s^{|m|})^2\begin{Bmatrix}J_{|m|}(k_s^{|m|}r)\\ I_{|m|}(k_s^{|m|}r)\end{Bmatrix}, \end{aligned} \tag{32}$$

$$\nabla^2=\frac{1}{r}\frac{\partial}{\partial r}\left(r\frac{\partial}{\partial r}\right)+\frac{1}{r^2}\frac{\partial^2}{\partial\phi^2}+\frac{\partial^2}{\partial z^2}$$

to obtain

$$\begin{aligned} \nabla^2 W_s^{|m|}(r)\mathrm{e}^{\mathrm{i}m\phi}&=-(k_s^{|m|})^2\widehat{N}_s^{|m|}\\ &\cdot\Big[J_{|m|}(k_s^{|m|}r)-B_s^{|m|}I_{|m|}(k_s^{|m|}r)\Big]\mathrm{e}^{\mathrm{i}m\phi}. \end{aligned} \tag{33}$$

The constant $B_s^{|m|}$ can been determined from Eq. (30):

$$\begin{aligned} B_s^{|m|}&=-\frac{q^{|m|}(\lambda)J_{|m|}(\lambda)+\big[2-u_{|m|}(\lambda)\big]J'_{|m|}(\lambda)}{q^{|m|}(\lambda)I_{|m|}(\lambda)-u_{|m|}(\lambda)I'_{|m|}(\lambda)}\\ &=-\frac{p^{|m|}(\lambda)J'_{|m|}(\lambda)-u_{|m|}(\lambda)J_{|m|}(\lambda)}{p^{|m|}(\lambda)I'_{|m|}(\lambda)+\big[2-u_{|m|}(\lambda)\big]I_{|m|}(\lambda)} \end{aligned} \tag{34}$$

for $\lambda = k_s^{|m|}a$ and $r = a$. The characteristic equation can be obtained by rearranging Eq. (34), which leads to:

$$\begin{aligned} &\Big\{q^{|m|}(\lambda)J_{|m|}(\lambda)+\big[2-u_{|m|}(\lambda)\big]J'_{|m|}(\lambda)\Big\}\\ &\quad\cdot\Big\{p^{|m|}(\lambda)I'_{|m|}(\lambda)+\big[2-u_{|m|}(\lambda)\big]I_{|m|}(\lambda)\Big\}\\ &-\Big\{p^{|m|}(\lambda)J'_{|m|}(\lambda)-u_{|m|}(\lambda)J_{|m|}(\lambda)\Big\}\\ &\quad\cdot\Big\{q^{|m|}(\lambda)I_{|m|}(\lambda)-u_{|m|}(\lambda)I'_{|m|}(\lambda)\Big\}=0. \end{aligned} \tag{35}$$

B.2. The normalization constant

The following integrals are necessary to calculate the normalisation constant (cf. (McLachlan, 1955) Eqs (5.79) on p. 162, (6.107) on p. 164, and (7.131) on p. 166):

$$\begin{aligned} &\frac{2}{a^2}\int_0^a J_{|m|}^2(k_s^{|m|}r)r\,\mathrm{d}r=J'^2_{|m|}(\lambda)+\left(1-\frac{m^2}{\lambda^2}\right)J^2_{|m|}(\lambda),\\ &\frac{2}{a^2}\int_0^a I_{|m|}^2(k_s^{|m|}r)r\,\mathrm{d}r=-I'^2_{|m|}(\lambda)+\left(1+\frac{m^2}{\lambda^2}\right)I^2_{|m|}(\lambda), \end{aligned} \tag{36}$$

and (cf. (McLachlan, 1955) Eqs (6.108) on p. 164, (7.132), and (7.133) on p. 166):

$$\begin{aligned} &\frac{2}{a^2}\int_0^a I_{|m|}(k_s^{|m|}r)J_{|m|}(k_s^{|m|}r)r\,\mathrm{d}r\\ &\qquad=\frac{1}{\lambda}\Big[I'_{|m|}(\lambda)J_{|m|}(\lambda)-I_{|m|}(\lambda)J'_{|m|}(\lambda)\Big]. \end{aligned} \tag{37}$$

Based on Eq. (30), it can be shown that:

$$\begin{aligned} B_s^{|m|}I_{|m|}(\lambda)&=2L^{|m|}(\lambda)-J_{|m|}(\lambda),\\ B_s^{|m|}I'_{|m|}(\lambda)&=2H^{|m|}(\lambda)-J'_{|m|}(\lambda), \end{aligned} \tag{38}$$

where

$$\begin{aligned} L^{|m|}(\lambda)&=[Q^{|m|}(\lambda)]^{-1}\\ &\cdot\Big[u_{|m|}(\lambda)J_{|m|}(\lambda)-p^{|m|}(\lambda)J'_{|m|}(\lambda)\Big], \end{aligned} \tag{39}_1$$

$$H^{|m|}(\lambda) = [Q^{|m|}(\lambda)]^{-1} \cdot \left\{ q^{|m|}(\lambda) J_{|m|}(\lambda) + \Big[2 - u_{|m|}(\lambda)\Big] J'_{|m|}(\lambda) \right\}, \quad (39)_2$$

$$\begin{aligned} Q^{|m|}(\lambda) &= \widehat{Q}^{|m|}(\lambda) + 2u_{|m|}(\lambda), \\ \widehat{Q}^{|m|}(\lambda) &= q^{|m|}(\lambda) p^{|m|}(\lambda) - u^2_{|m|}(\lambda), \end{aligned} \quad (39)_3$$

Applying Eq. (38) to Eq. (28) gives the following result:

$$\begin{aligned} (\widehat{N}_s^{|m|})^{-2} = {} & \left(1 + \frac{m^2}{\lambda^2}\right)\Big[2L^{|m|}(\lambda) - J_{|m|}(\lambda)\Big]^2 \\ & + \left(1 - \frac{m^2}{\lambda^2}\right) J^2_{|m|}(\lambda) \\ & - 4H^{|m|}(\lambda)\Big[H^{|m|}(\lambda) - J'_{|m|}(\lambda)\Big] \\ & + \frac{4}{\lambda}\Big[H^{|m|}(\lambda) J_{|m|}(\lambda) - L^{|m|}(\lambda) J'_{|m|}(\lambda)\Big], \end{aligned} \quad (40)$$

where for $\lambda = k_s^{|m|} a$ (cf. Eq. (28)).

B.3. The spectral density of the eigenfunction

The spectral density of the plate's eigenfunction can be obtained in its explicit form by calculating the integral in Eq. $(27)_2$, which leads to (cf. Eq. (24)):

$$\widehat{D}_s^{|m|}(\tau) = \widehat{N}_s^{|m|}\Big[\widehat{I}_{G,s}^{|m|}(\tau) + B_s^{|m|}\widehat{I}_{F,s}^{|m|}(\tau)\Big], \quad (41)$$

where

$$\begin{aligned} \widehat{I}_{G,s}^{|m|}(\tau) &= \int_0^a J_{|m|}(k_s^{|m|} r) J_{|m|}(\tau r) r \, \mathrm{d}r, \\ \widehat{I}_{F,s}^{|m|}(\tau) &= \int_0^a I_{|m|}(k_s^{|m|} r) J_{|m|}(\tau r) r \, \mathrm{d}r. \end{aligned} \quad (42)$$

Now, the integral formulas for the cylindrical functions, the modified Bessel function, and the MacDonald function can be used directly (cf. (McLachlan, 1995) Eqs (5.72) on p. 162, (6.108) on p. 164, and (7.132) on p. 166):

$$\begin{aligned} \widehat{I}_{G,s}^{|m|}(\tau) &= \frac{a}{(k_s^{|m|})^2 - \tau^2} \cdot \Big[\tau J_{|m|}(\lambda) J'_{|m|}(\tau a) - k_s^{|m|} J'_{|m|}(\lambda) J_{|m|}(\tau a)\Big], \\ \widehat{I}_{F,s}^{|m|}(\tau) &= \frac{a}{(k_s^{|m|})^2 + \tau^2} \cdot \Big[k_s^{|m|} I'_{|m|}(\lambda) J_{|m|}(\tau a) - \tau I_{|m|}(\lambda) J'_{|m|}(\tau a)\Big] \end{aligned} \quad (43)$$

for $\lambda = k_s^{|m|} a$. Finally, implementing Eqs (38) and (43), in Eq. (42) gives the spectral density in the form of:

$$\widehat{D}_s^{|m|}(\tau) = \frac{2\widehat{N}_s^{|m|}}{(k_s^{|m|})^2 + \tau^2} \cdot \left[\frac{(k_s^{|m|})^2}{(k_s^{|m|})^2 - \tau^2} \widehat{\psi}_s^{|m|}(k_s^{|m|} a, \tau a) + \widehat{\phi}_{a,s}^{|m|}(k_s^{|m|} a, \tau a)\right], \quad (44)$$

where

$$\begin{aligned} \widehat{\psi}_s^{|m|}(u, v) &= -u J'_{|m|}(u) J_{|m|}(v) + v J_{|m|}(u) J'_{|m|}(v), \\ \widehat{\phi}_{r,s}^{|m|}(u, v) &= u H^{|m|}(u) J_{|m|}(v) - v L^{|m|}(u) J'_{|m|}(v). \end{aligned} \quad (45)$$

It can also be shown that the spectral density in Eq. (44) is singular for $\tau = k_s^{|m|}$. Therefore, the following limit has been calculated from Eq. $(27)_2$ (cf. Eq. (24) and (42)):

$$\lim_{\tau \to k_s^{|m|}} \widehat{D}_s^{|m|}(\tau) = \widehat{D}_s^{|m|}(k_s^{|m|}) = \widehat{N}_s^{|m|}\Big[\widehat{I}_{G,s}^{|m|}(k_s^{|m|}) + B_s^{|m|}\widehat{I}_{F,s}^{|m|}(k_s^{|m|})\Big]. \quad (46)$$

Now, the integrals can be expressed as follows (cf. (McLachlan, 1995) Eqs (5.80) on p. 162, (6.108) on p. 164, and (7.132) on p. 166):

$$\begin{aligned} \widehat{I}_{G,s}^{|m|}(k_s^{|m|}) &= \frac{a^2}{2} \cdot \left[\left(1 - \frac{m^2}{(k_s^{|m|} a)^2}\right) J_{|m|}(k_s^{|m|} a) J_{|m|}(k_s^{|m|} a) + J'_{|m|}(k_s^{|m|} a) J'_{|m|}(k_s^{|m|} a)\right], \\ B_s^{|m|}\widehat{I}_{F,s}^{|m|}(k_s^{|m|}) &= \frac{a}{k_s^{|m|}} \cdot \Big[H^{|m|}(k_s^{|m|} a) J_{|m|}(k_s^{|m|} a) - L^{|m|}(k_s^{|m|} a) J'_{|m|}(k_s^{|m|} a)\Big]. \end{aligned} \quad (47)$$

References

1. Abramowitz M., Stegun I. [Eds] (1972), *Handbook of Mathematical Functions with Formulas, Graphs, and Mathematical Tables*, U.S. Department of Commerce, National Bureau of Standards.
2. Arenas J. (2009), On the sound radiation from a circular hatchway, *International Journal of Occupational Safety and Ergonomics*, **15**(4): 401–407, doi: 10.1080/1080 3548.2009.11076819.
3. Arenas J., Ugarte F. (2016), A note on a circular panel sound absorber with an elastic boundary condition, *Applied Acoustics*, **114**: 10–17, doi: 10.1016/j.apacoust.2016.07.002.
4. Cho D., Kim B., Kim J.H., Choi T., Vladimir N. (2016), Free vibration analysis of stiffened panels with lumped mass and stiffness attachments, *Ocean Engineering*, **124**: 84–93, doi: 10.1016/j.oceaneng.2016.07.055.

5. Hasheminejad S.M., Keshavarzpour H. (2016), Robust active sound radiation control of a piezo-laminated composite circular plate of arbitrary thickness based on the exact 3D elasticity model, *Journal of Low Frequency Noise Vibration and Active Control*, **35**(2): 101–127, doi: 10.1177/0263092316644085.
6. Hasheminejad S.M., Shakeri R. (2017), Active transient acousto-structural response control of a smart cavity-coupled circular plate system, *Archives of Acoustics*, **42**(2): 273–286, doi: 10.1515/aoa-2017-0030.
7. Jandak V., Svec P., Jiricek O., Brothanek M. (2017), Piezoelectric line moment actuator for active radiation control from light-weight structures, *Mechanical Systems and Signal Processing*, **96**: 260–272, doi: 10.1016/j.ymssp.2017.04.003.
8. Jun K., Eom H. (1995), Acoustic scattering from a circular aperture in a thick hard screen, *The Journal of the Acoustical Society of America*, **98**(4): 2324–2327, doi: 10.1121/1.414404.
9. Leissa A. (1969), *Vibration of Plates*, National Aeronautics and Space Administration, Washington D.C., http://ntrs.nasa.gov/search.jsp?R=19700009156.
10. Lovat G. *et al.* (2019), Shielding of a perfectly conducting circular disk: Exact and static analytical solution, *Progress In Electromagnetics Research C*, **95**: 167–182, doi: 10.2528/pierc19052908.
11. McLachlan N. (1955), *Bessel Functions For Engineers*, Clarendon Press, Oxford.
12. Ostachowicz W., Krawczuk M., Cartmell M. (2002), The location of a concentrated mass on rectangular plates from measurements of natural vibrations, *Computers and Structures*, **80**(16–17): 1419–1428, doi: 10.1016/S0045-7949(02)00084-6.
13. Pierce A. (1994), *Acoustics. An Introduction to Its Physical Principles and Applications*, Acoustical Society of America through American Institute of Physics, New York.
14. Rao S. (2007), *Vibrations of Continuous Systems*, Wiley, New Jersey.
15. Rayleigh J. (1896), *The Theory of Sound*, Volume 2, 2nd ed., Macmillan, New York.
16. Rdzanek W.P. (2018), Sound radiation of a vibrating elastically supported circular plate embedded into a flat screen revisited using the Zernike circle polynomials, *Journal of Sound and Vibration*, **434**: 92–125, doi: 10.1016/j.jsv.2018.07.035.
17. Rdzanek W.P., Engel Z. (2000), Asymptotic formulas for the acoustic power output of a clamped annular plate, *Applied Acoustics*, **60**(1): 29–43, doi: 10.1016/S0003-682X(99)00041-9.
18. Rdzanek W.P., Rdzanek W.J., Engel Z., Szemela K. (2007), The modal low frequency noise of an elastically supported circular plate, *International Journal of Occupational Safety and Ergonomics*, **13**(2): 147–157, doi: 10.1080/10803548.2007.11076718.
19. Rdzanek W.P., Szemela K. (2019), Sound radiation by a vibrating annular plate using radial polynomials and spectral mapping, *The Journal of the Acoustical Society of America*, **146**(4): 2682–2691, doi: 10.1121/1.5130193.
20. Sommerfeld A. (1964), *Partial Differential Equations in Physics*, Academic Press, New York.
21. Trojanowski R., Wiciak J. (2012), Comparison of efficiency of different shapes of homogeneous and two-part piezo elements on vibration reduction, *Acta Physica Polonica A*, **122**(5): 905–907, doi: 10.12693/APhysPolA.122.905.
22. Trojanowski R., Wiciak J. (2020), Impact of the size of the sensor part on sensor-actuator efficiency, *Journal of Theoretical and Applied Mechanics*, **58**(2): 391–401, doi: 10.15632/jtam-pl/118948.
23. Wiciak J., Trojanowski R. (2015), Evaluation of the effect of a step change in piezoactuator structure on vibration reduction level in plates, *Archives of Acoustics*, **40**(1): 71–79, doi: 10.1515/aoa-2015-0009.
24. Williams E., (1999), *Fourier Acoustics. Sound Radiation and Nearfield Acoustical Holography*, Academic Press, London.
25. Wrona S., Pawelczyk M., Cheng L. (2021a), A novel semi-active actuator with tunable mass moment of inertia for noise control applications, *Journal of Sound and Vibration*, **509**: 116244, doi: 10.1016/j.jsv.2021.116244.
26. Wrona S., Pawelczyk M., Cheng L. (2021b), Semi-active links in double-panel noise barriers, *Mechanical Systems and Signal Processing*, **154**: 107542, doi: 10.1016/j.ymssp.2020.107542.
27. Wrona S., Pawelczyk M., Qiu X. (2020), Shaping the acoustic radiation of a vibrating plate, *Journal of Sound and Vibration*, **476**: 115285, doi: 10.1016/j.jsv.2020.115285.
28. Zagrai A., Donskoy D. (2005), A "soft table" for the natural frequencies and modal parameters of uniform circular plates with elastic edge support, *Journal of Sound and Vibration*, **287**(1–2): 343–351, doi: 10.1016/j.jsv.2005.01.021.